공학석사 학위논문

Oxidative chlorination of methane over Fe_2O_3/CeO_2 catalyst

Fe_2O_3/CeO_2 촉매를 이용한 메탄의 산화염소화반응

2018 년 8 월

서울대학교 대학원

화학생물공학부

김 정 은

Oxidative chlorination of methane over Fe_2O_3/CeO_2 catalysts

지도교수 김 도 희

이 논문을 공학석사 학위논문으로 제출함

2018 년 8 월

서울대학교 대학원

화학생물공학부

김 정 은

김정은의 공학석사 학위논문을 인준함

2018 년 8 월

위 원 장 이 종 민 (인)

부위원장 김 도 희 (인)

위 원 이 원 보 (인)

Abstract

Oxidative chlorination of methane over Fe_2O_3/CeO_2 catalysts

Jeongeun Kim

Chemical and Biological Engineering

The Graduate School

Seoul National University

Methane, which accounts for higher than 80% of natural gas components, is an abundant alternative feedstock to petroleum. However, efficient utilization of methane especially for chemical production has been challenging task in catalysis community due to the highly stable C–H bonds of methane. Although there are commercialized methane activation processes such as steam–

reforming, partial oxidation and auto-thermal reforming, they are disadvantageous in the terms of capital and energy.

Methane activation through oxychlorination is in the spotlight due to the relatively mild reaction conditions at atmospheric pressure and in the temperature range of 450-550 ℃. CeO_2 is known to exhibit good activity for oxychlorination which is arising from its redox properties ($Ce^{4+} \leftrightarrow Ce^{3+}$), however, significant amounts of by-products such as CO_2, CO and carbon deposits are produced during the reaction over CeO_2. At 510 ℃, where the yield of chlorinated products is maximized, the selectivity of 56.8% for chloromethane (CM) and 17.2% for dichloromethane (DCM) are obtained, while by-products (CO_2, CO and carbon deposits) are produced with about 26% selectivity.

In this study, various metals were introduced into CeO_2 to promote the activity of CeO_2 for methane oxychlorination. Metal/CeO_2 catalysts were prepared by applying wet impregnation method, and all catalysts were calcined at 600 ℃ for 6 hours. From the result of activity test, iron showed the best promoting effect on CeO_2 for methane oxychlorination, and thus, the effect of iron in Fe_2O_3/CeO_2 catalysts on methane oxychlorination were extensively studied. The activity test result of Fe_2O_3/CeO_2 with different iron loading shows

that although there are no advantages in the perspective of methane conversion, the production of by-products is suppressed by adding iron irrespective of iron loading. Fe_2O_3/CeO_2 with 3 wt% iron shows the maximum yield at 510 ℃ with 23% conversion of methane and 65% selectivity of chloromethane. To clarify the cause of the promotion by addition of iron, the characterizations of catalysts, e.g. XPS, BET, XRD, TEM and H_2 TPR, were conducted. XRD and H_2 TPR results indicate that iron-cerium solid solution is formed, resulting in the production of more easily reduced cerium oxide. In addition, the suppression of catalyst sintering during the reaction is confirmed by XRD and TEM. Consequently, the selectivity of by-products decreases more significantly over Fe_2O_3/CeO_2 than over cerium oxide which can be attributed to the facilitation of HCl oxidation arising from the enhanced reducibility of the former sample.

Keywords : Methane activation, Oxidative chlorination, CeO_2, Suppression of CO and CO_2, Chloromethane.

Student Number : 2016-21017

Contents

List of Tables

List of Figures

Chapter 1. Introduction

1.1. Background of methane activation

Natural gas, which has affluent proven reserves all over the world, is considered as an attractive alternative to petroleum due to its cost-competitiveness and environmental-friendliness [1-6]. According to the International Energy Outlook 2016 from U.S. Energy Information Administration (EIA), the world-wide annual consumption of natural gas will reach 5,680 billion cubic meters (bcm) in 2040 from 3,360 bcm in 2012 [7]. The importance of natural gas as a chemical feedstock is particularly significant because the other alternative resources, such as solar, wind, geothermal and nuclear, can only be used for electricity production.

However, there are some drawbacks for unconstrained utilization of natural gas. Significant percentage of proven natural gas remain stranded in remote location from the market [5, 8], and thus, the technologies to convert natural gas into liquid hydrocarbons are required for convenient transportation and storage. Production of valuable chemicals from methane, which accounts for most of the

natural gas components [9, 10], however, is challenging issue due to the four highly stable C–H bonds ($\Delta H_d = 440\ kJ\ mol^{-1}$) in methane [4]. Furthermore, 150 bcm of natural gas which are about 5% of world-wide annual consumption are just flared or vented into atmosphere [11]. It can cause serious environmental problems because methane has 21 times more global warming potential than the same amount of carbon dioxide [1, 12]. For these reasons, the effective conversion of natural gas especially methane has been intensively studied in the catalysis community [2–5, 8, 13], whereas currently less than 10% of natural gas are used as chemical feedstock [4].

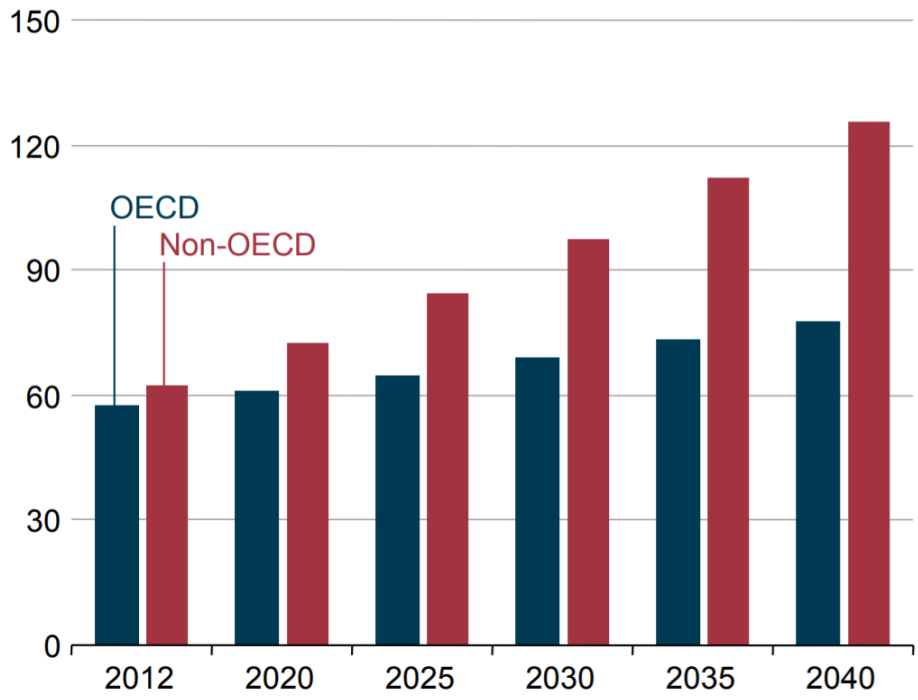

Figure. 1-1. World natural gas consumption, 2012-40 (trillion cubic feet) [7].

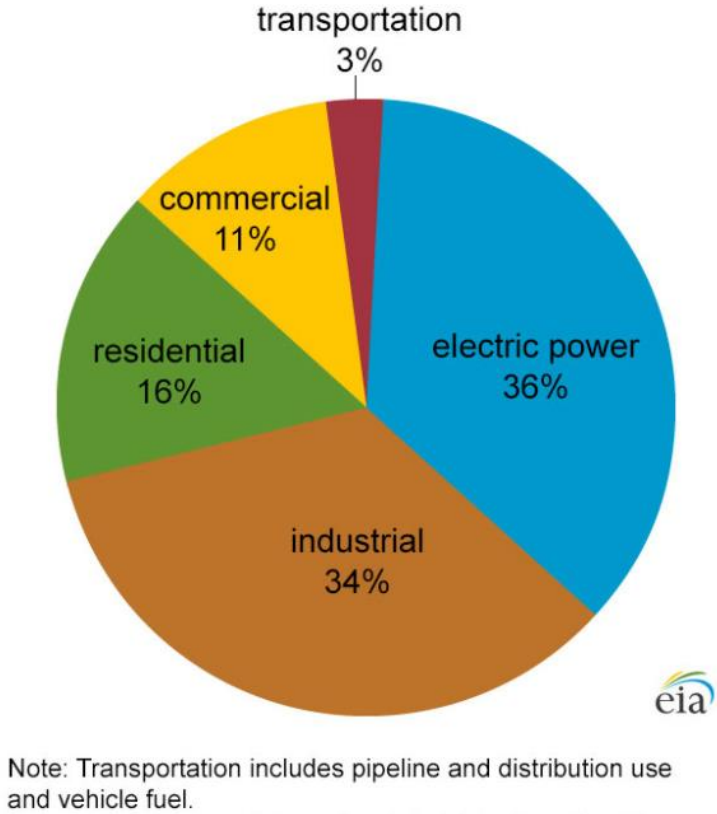

Figure. 1-2. U.S. natural gas consumption by sector, 2016 (Total=27.5 trillion cubic feet) [14].

1.2. Oxidative halogenation

Methane activation processes, e.g. partial oxidation, steam reforming and auto-thermal reforming, were commercialized, but there are limitations that those processes are capital- and energy-intensive [4, 15]. Although the various other methods of activating methane, e.g. OCM (oxidative coupling of methane), catalytic methane aromatization and CO_2 reforming, have been studied, products yield and process cost do not achieve the economic criteria to be commercialized.

Halogen mediated methane activation has been considered as an attractive process because of the mild operating temperature in the range of 450-550 ℃ [4, 16-22]. Methyl halides produced in the methane halogenation process are the platform materials for manufacturing a variety of valuable chemicals, for instance, methanol, acetic acid, dimethyl ether and C_8-C_{13} aromatics etc. [3]. Chlorine and bromine are mainly used as halogen source [2-4, 23-28]. Methane halogenation using gaseous halogen is known to occur according to the following reactions.

$$CH_4 + Br_2 \rightarrow CH_3Br + HBr, \quad (\Delta H_r^\circ\,(298\ \mathrm{K}) = -27.597\ \mathrm{kJ\ mol^{-1}})$$

$$CH_4 + Cl_2 \rightarrow CH_3Cl + HCl, \quad (\Delta H_r^\circ\,(298\ K) = -101.18\ kJ\ mol^{-1})$$

These reactions have a limitation in that a process to regenerate X_2 from the produced HX is required. On the other hand, the oxidative halogenation of methane using O_2 and HX has the advantages of being thermodynamically more favorable than the gaseous halogenation described above and requiring no additional regeneration process [29]. Theoretically methane oxidative halogenation occurs in the following reactions.

$$CH_4 + HBr + 1/2O_2 \rightarrow CH_3Br + H_2O, \ (\Delta H_r^\circ\,(298\ K) = -165.71\ kJ\ mol^{-1})$$

$$CH_4 + HCl + 1/2O_2 \rightarrow CH_3Cl + H_2O, \ (\Delta H_r^\circ\,(298\ K) = -158.38\ kJ\ mol^{-1})$$

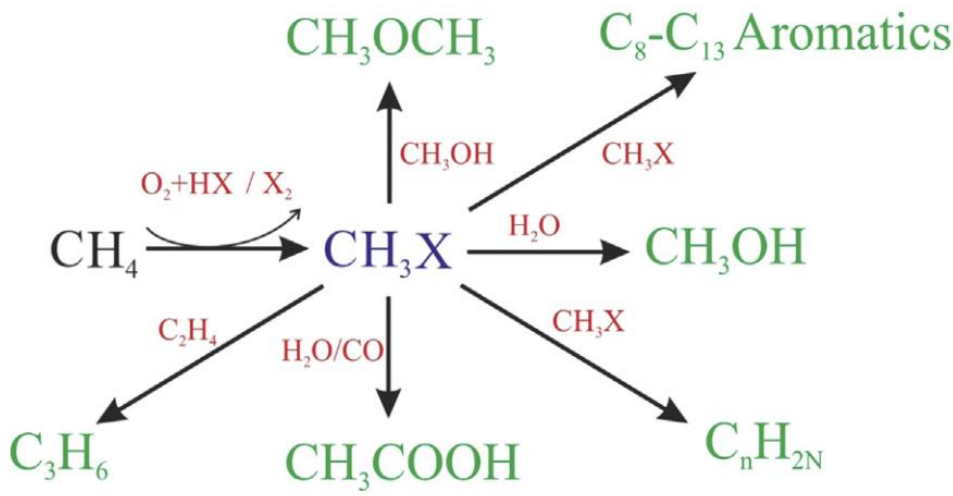

Figure. 1-3. CH_4 conversion into value added products via halogenation [3].

1.3. Objectives

The use of HCl as a halogen source has its advantages because the cost of HCl is lower compared to HBr and the technology and infrastructure of the process using HCl, such as the VCM production process, are already exist [23, 30]. However, chlorination is less selective than bromination, and previous research about methane oxidative chlorination has not been well conducted yet compared to oxidative bromination [23].

Some categories of catalysts, e.g. copper based catalysts, metal oxychloride, metal oxide and metal phosphate, have been proposed for oxidative chlorination of methane [23]. Among them, CeO_2, which exhibits good activity arising from the Ce^{4+}/Ce^{3+} redox property, has recently attracted attention. The redox property of Ce^{4+}/Ce^{3+} plays a key role in the HCl oxidation to produce activated Cl species for methane oxidative chlorination [23, 29–34]. Despite the excellent activity of CeO_2, CO and CO_2 are generated as unwanted products from side reactions (additional chlorination and oxidation of produced chloromethane). Accordingly, there is need to study a way for suppressing side reactions.

In this study, the effects of various metals on reactivity of CeO_2

for methane oxidative chlorination were investigated. In particular, various wt% of iron was impregnated in CeO_2 in order to suppress the production of unwanted products (CO and CO_2) and to promote the selective production of chlorinated products. Furthermore, the effects of iron on redox property and lattice structure of CeO_2 were studied to explicate the outstanding activity of Fe_2O_3/CeO_2.

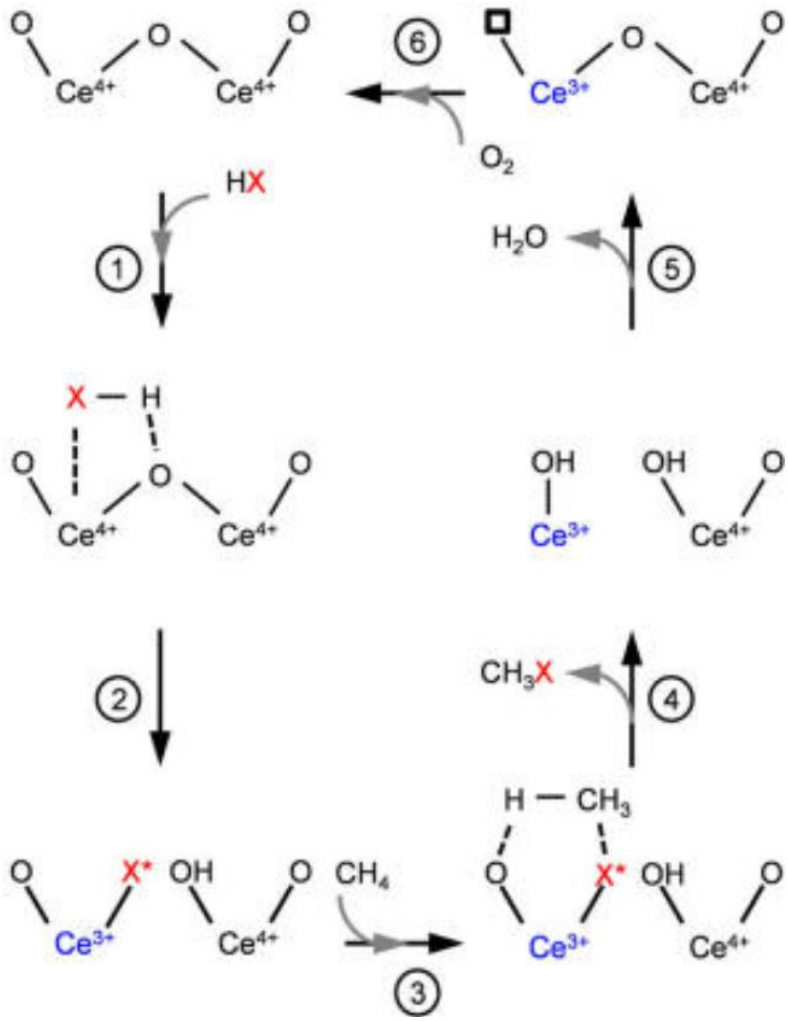

Figure. 1-4. Proposed reaction pathway for the methane oxidative halogenation over CeO_2 [23].

Chapter 2. Experimental

2.1. Catalysts preparation

CeO_2 was obtained from Rhodia® and metal precursors were purchased from Sigma Aldrich (Fe, Mn and Co), Alfa Aesar (Ni, Ag, Y, Nd, and Eu), and Samchun Chemicals (La). Metal/CeO_2 catalysts (Metal= Fe, Mn, Co, Ni, Ag, Y, Nd, Eu and La) were prepared by wet impregnation. CeO_2 was immersed in an aqueous solution of metal precursor ($Fe(NO_3)_3 \cdot 9H_2O$, $Mn(NO_3)_2 \cdot 4H_2O$, $Co(NO_3)_2 \cdot 6H_2O$, $Ni(NO_3)_2 \cdot 6H_2O$, $AgNO_3$, $Y(NO_3)_3 \cdot 6H_2O$, $Nd(NO_3)_3 \cdot 6H_2O$, $Eu(NO_3)_3 \cdot 6H_2O$ and $LaCl_3 \cdot 7H_2O$) and stirred for 1 hour. Solvent was removed by using rotary evaporator and the catalysts were dried at 373 K overnight. All catalysts were calcined under air using a muffle furnace at 600 ℃ for 6 hours. The prepared samples were denoted as metal(x)/CeO_2, which represents x wt% of metal loading.

2.2. Catalysts characterization

2.2.1. XPS

X-ray photoelectron spectroscopy (XPS) analysis was carried out using a K-alpha (Thermo VG, U.K.) equipped with Al Kα X-ray source (hν = 1486.6 eV). The samples were degassed at room temperature overnight and the vacuum pressure during analysis was about 10^{-9} mb. To eliminate the effect of charging, the spectra were corrected with a binding energy of C 1s (284.6 eV) [35, 36].

2.2.2. BET

The specific surface area of samples were investigated by N_2 adsorption-desorption isotherm at 77 K using Micrometrics ASAP 2010. Prior to the measurement, pretreatment of the samples was carried out at 250 ℃ for more than 5 hours. Brunauer-Emmett-Teller (BET) method was used to calculate the specific surface area of the samples.

2.2.3. XRD

X-ray diffraction (XRD) patterns of the samples were obtained with Ultra X18 (Rigaku Corp.) at 30 mA and 40 kV using Cu Kα radiation. The measurements were conducted with a scanning step size of 0.02° from 10° to 80° (2θ). Debye-Scherrer equation was used to calculate the crystallite size.

2.2.4. TEM

Transmission electron microscope (TEM) images captured by using JEM-2100F (TEM, JEOL., Japan) were used to analyze the particles in the samples. The sample dispersed in absolute ethanol was dropped onto a carbon-coated Cu grid and then dried at room temperature. Accelerating voltage for analysis was 200 kV.

2.2.5. H_2 TPR

H_2 temperature programmed reduction (H_2 TPR) analysis was conducted on a BEL CAT (MicrotracBEL Corp.) with a thermal conductivity detector (TCD). For the measurement, the samples were pretreated under air condition at 400 ℃ for 1 hour and cooled

down to 40 ℃. After that, the reduction of samples with 5% H_2/Ar was progressed until the temperature reached 900 ℃ at the rate of 10 ℃/min.

2.3. Catalytic properties for methane oxychlorination

2.3.1. Activity test

The Catalytic activity tests were carried out using 0.1 g catalysts at the temperature of 450 ℃ to 550 ℃, which was controlled with thermocouples located at the furnace and directly above the catalyst bed. For activity tests, all catalysts were sieved in 0.18–0.25 mm and then loaded in a fixed bed quartz tubular reactor. Total feed flow including internal standard (N_2), diluent (Ar), and reactants (CH_4, O_2 and HCl) was set as 50 ml/min, and the volume ratio of component was N_2:Ar:CH_4:O_2:HCl =10:3:4:1:2. The outlet stream was maintained at 150 ℃ to prevent condensation of the products. After the activity test and analysis with online gas chromatograph, the gas stream was neutralized via NaOH trap and vented.

2.3.2. Analytical method

Quantitative analysis of outlet gas stream was performed with online gas chromatograph (Agilent Technologies 6890N / G1530N with Carboxen 1000 packed column and HP Plot–Q capillary column). N_2, O_2, CH_4, CO and CO_2 were analyzed with thermal conductivity

detector (TCD) and CH_4, CH_3Cl (Chloromethane; CM), CH_2Cl_2 (Dichloromethane; DCM) and $CHCl_3$ (Trichloromethane; TCM) were analyzed with flame ionization detector (FID). Since methane oxidative chlorination proceeds with a change in the mole number, all data from gas chromatograph should be corrected with internal standard factor, α. The internal standard factor was obtained as follows, where $n(N_2)$ is the number of mole of N_2.

$$\alpha = \frac{n(N_2)^{inlet}}{n(N_2)^{outlet}}$$

The conversion of methane ($X(CH_4)$) was obtained by using the following equation, where $n(CH_4)$ is the number of mole of methane.

$$X(CH_4) = \frac{n(CH_4)^{inlet} - \alpha \times n(CH_4)^{oulet}}{n(CH_4)^{inlet}} \times 100, \%$$

The selectivity (S) and yield (Y) were calculated from the basis of carbon according to the following equations, where n(j) is the number of mole of j component (j: CM, DCM, TCM, CO or CO_2) [29].

$$S(j) = \frac{n(j)^{outlet}}{\sum n(j)^{outlet}} \times 100, \%$$

$$Y(j) = X(CH_4) \times S(j), \%$$

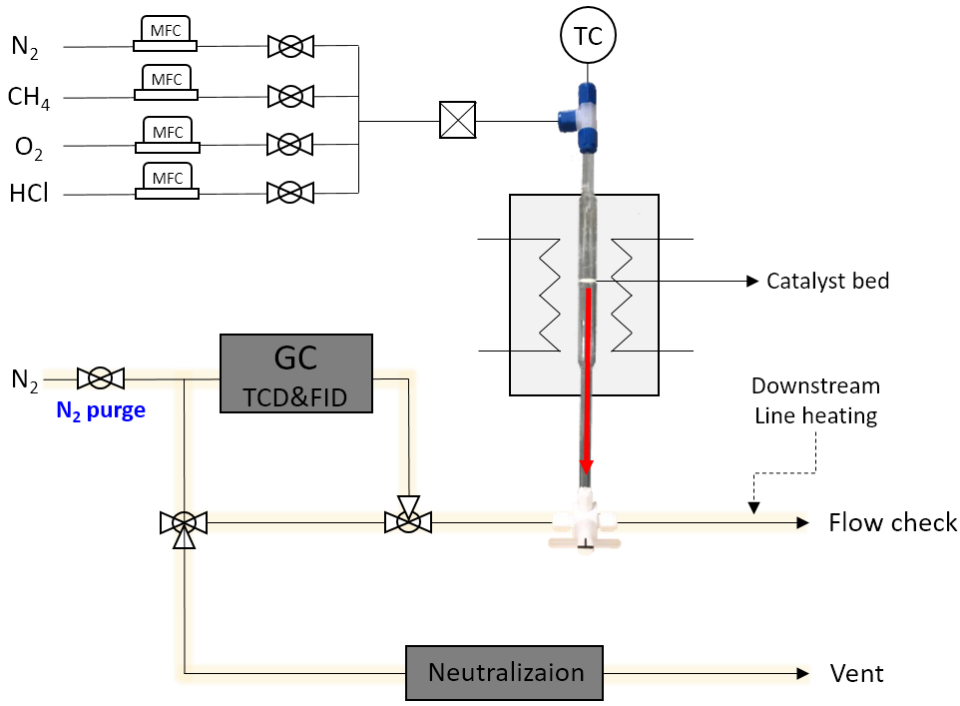

Figure. 2-1. Scheme of reaction system.

Chapter 3. Result and Discussion

3.1. Catalytic properties for methane oxychlorination

The catalytic activity of CeO_2 for methane oxidative chlorination as a function of temperature is presented in Figure. 3-1. During the reaction, methane activation proceeds to produce chlorinated products (CM, DCM and TCM), and by-products (CO and CO_2) are produced through side reaction. The selectivity of CM is 84.6% at 450 ℃, and decreases as the temperature increases. On the other hand, for DCM the selectivity reaches a maximum value of 21.1% at 480 ℃ and the selectivity of side reaction products (CO and CO_2) gradually increases with increasing temperature. It is known that the produced CM is further chlorinated and the decomposition of chlorinated products into CO or CO_2 occurs, during the oxidative chlorination of methane [11]. Correspondingly, the further chlorination of CM to DCM or TCM is facilitated on CeO_2 with an increment of temperature. In addition, the oxidation of carbon containing materials to CO and CO_2 is observed above 480 ℃, and thus the selectivity of DCM is maximized at that temperature. Depending on the trade-off relationship between selectivity and

conversion, the yield of chlorinated products (CM, DCM and TCM) shows a maximum value at 510 ℃ with the selectivity of 56.8% and 17.2% for CM and DCM, respectively, and methane conversion of 23.6%. At that temperature, the selectivity of CO and CO_2 are 18.5% and 7.2%, respectively.

Figure. 3-2 shows the activity of the metal(3)/CeO_2 for oxidative chlorination of methane at 510 ℃. The activation of methane is significantly lower over Co(3)/ CeO_2, Ni(3)/CeO_2 and Ag(3)/CeO_2 than over CeO_2. When rare-earth metals (Y, Nd, Eu and La) are supported on CeO_2, the production of by-products (CO and CO_2) is suppressed, but there is no significant difference in the yield of chlorinated products. In the case of Fe_2O_3(3)/CeO_2, the effect of metal impregnation is conspicuous. The yield of chlorinated products increases and the yield of by-products (CO and CO_2) decreases. Especially, the production of CO_2, low value-added, is suppressed, and the desired product, CM, is produced with high selectivity (Y(CO+CO_2)=2.8% and Y(CM+DCM)=19.7%). Hence, the effects of Fe on the properties of CeO_2 were investigated more deeply.

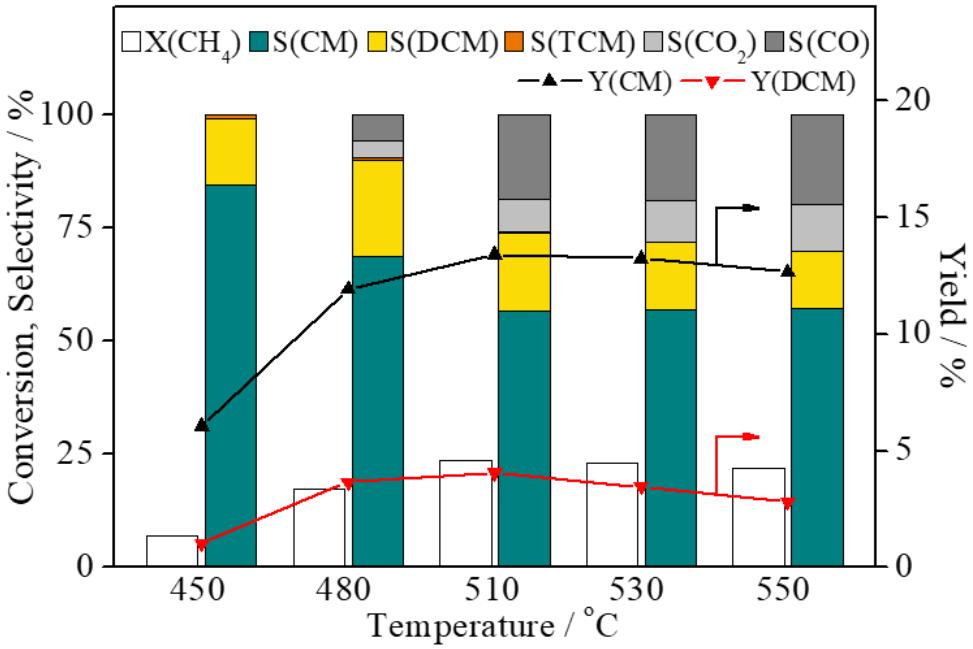

Figure. 3-1. Catalytic activity of CeO_2 for oxidative chlorination of methane as a function of temperature.

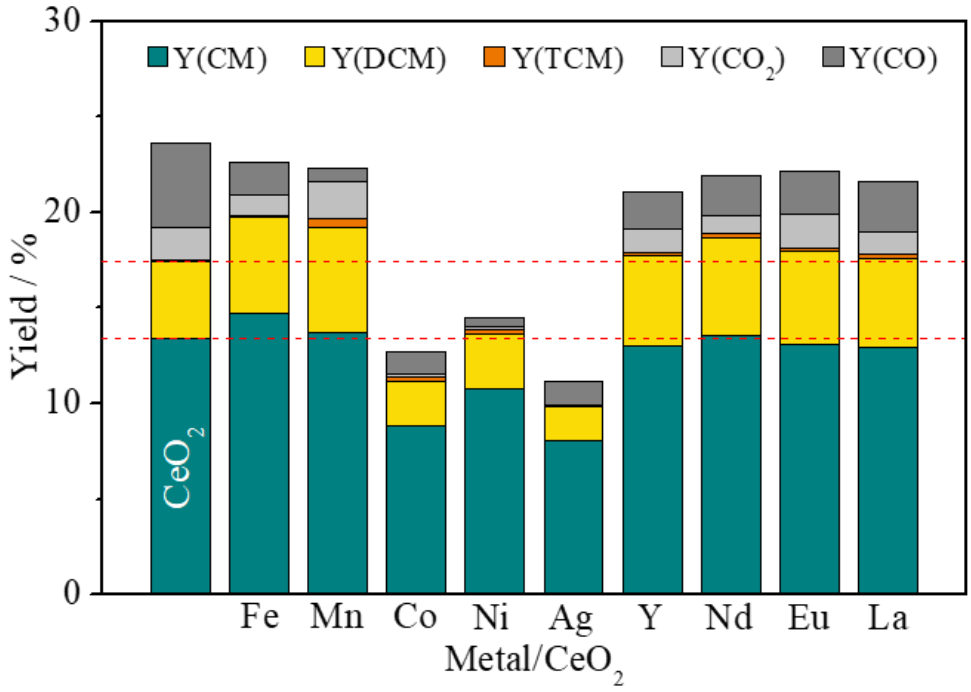

Figure. 3-2. Catalytic activity of metal(3)/CeO_2 for oxidative chlorination of methane at 510 ℃.

The catalytic activity of Fe_2O_3/CeO_2 according to Fe loading is shown in Figure. 3-3. In terms of methane conversion, there is no advantage in introducing Fe into CeO_2. However, at comparable methane conversion, the selectivity of by-products (CO and CO_2) decreases significantly. Especially, CO_2 is rarely generated over $Fe_2O_3(4)/CeO_2$ and $Fe_2O_3(6)/CeO_2$. Consequently, chlorinated products are produced with high selectivity by introducing Fe regardless of loading amounts. The yield of chlorinated products shows the highest value of about 20.0% over $Fe_2O_3(3)/CeO_2$, with CM and DCM selectivity of 65.2% and 22.0%, respectively. At the same time, the CO selectivity of 7.8% and CO_2 selectivity of 4.6% are attained, whereas those over CeO_2 are obtained as 18.5% and 7.2% at the same temperature. It can be summarized that the introduction of Fe into CeO_2 increases the selectivity of chlorinated products by suppressing the production of by-products (CO and CO_2), and thus, the chlorinated products produce with maximum yield over $Fe_2O_3(3)/CeO_2$.

The catalytic properties of $Fe_2O_3(3)/CeO_2$ accordance with temperature are exhibited in Figure. 3-4. As with the tendency over CeO_2, the selectivity of by-products (CO and CO_2) increases with increasing temperature, but the values are lower than that over CeO_2

at all temperatures. In addition, unlike over CeO_2, the selectivity of CM increases at over 510 ℃, which seems to be due to Fe. As a trade-off relationship of selectivity and conversion, the yield of CM and DCM are maximized at 510 ℃, like over CeO_2, as 14.8% and 5.0%, respectively.

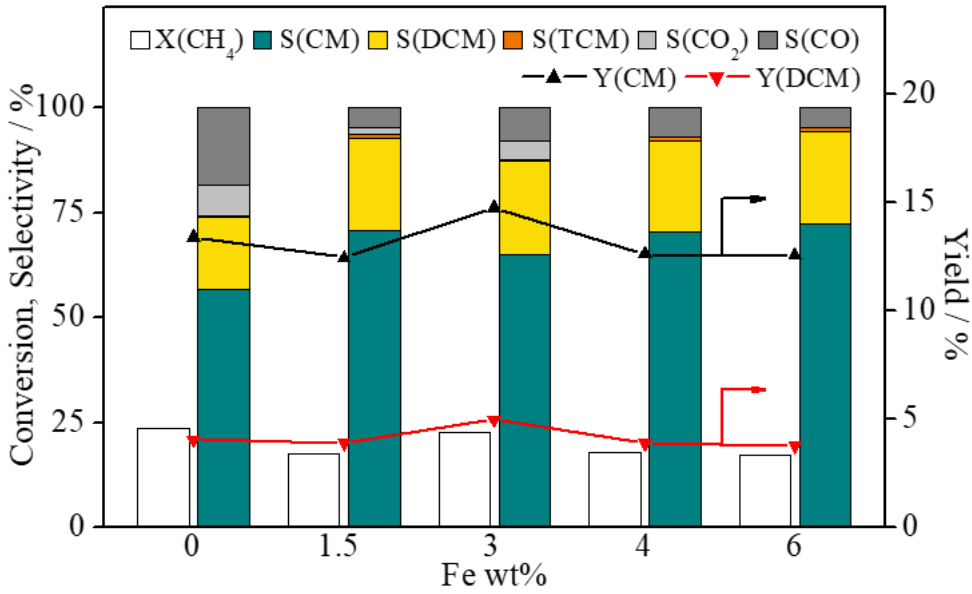

Figure. 3-3. Catalytic activity of Fe_2O_3(x)/CeO_2 for oxidative chlorination of methane at 510 ℃ according to Fe loading.

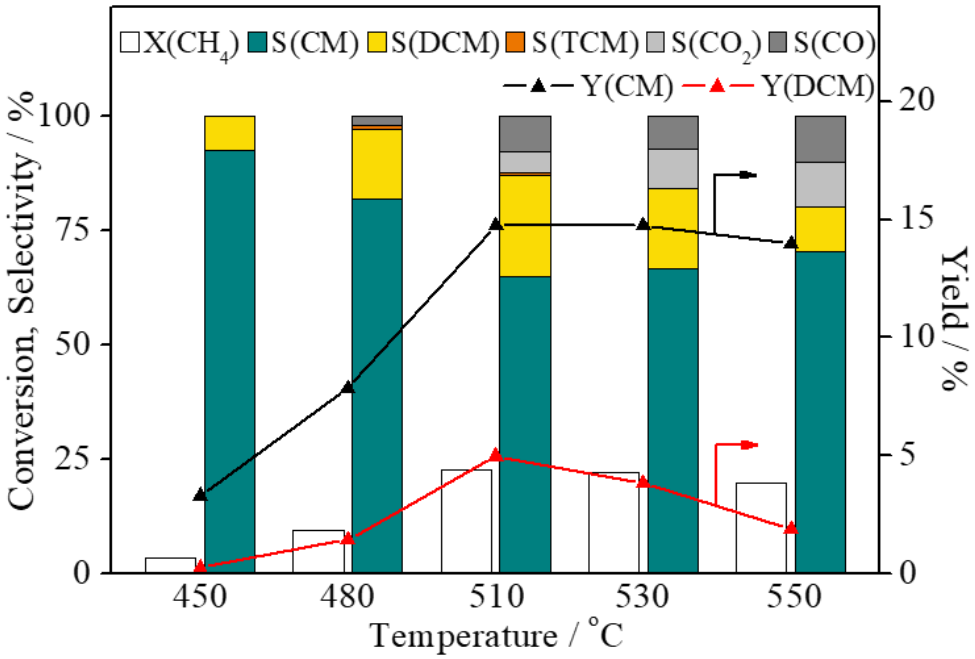

Figure. 3-4. Catalytic activity of Fe_2O_3(3)/CeO_2 for oxidative chlorination of methane as a function of temperature.

3.2. XPS

Ce 3d X-ray photoelectron spectra (XPS) of Fe_2O_3(3)/CeO_2 before and after reaction are displayed in Figure. 3-5. Ce 3d spectra present eight peaks which are accordance with Ce^{4+} and Ce^{3+}. The three pairs of peaks labeled as v/u, v"/u", and v"'/u"' are arising from Ce^{4+} contributions and v'/u' from Ce^{3+} [37]. There are no significant differences between fresh and used sample in Ce 3d photoelectron spectra.

Figure. 3-6 shows Fe 2p XP spectra of CeO_2 and Fe_2O_3(3)/CeO_2. As can be seen in Figure. 3-6(a), the Auger peaks of Ce are obtained at 732.3 eV and 716.9 eV near the binding energy at which the Fe 2p satellite peaks are observed [35, 38]. Hence, it is hard to distinguish the satellite peaks of Fe 2p in Figure. 3-6(b). The peaks at 723.6 eV and 710.9 eV correspond to the main Fe $2p_{1/2}$ and Fe $2p_{3/2}$ of Fe_2O_3, respectively [38-42]. The intensity of the main Fe 2p peaks decreases after the reaction, which means a decrease in the relative surface concentration of Fe.

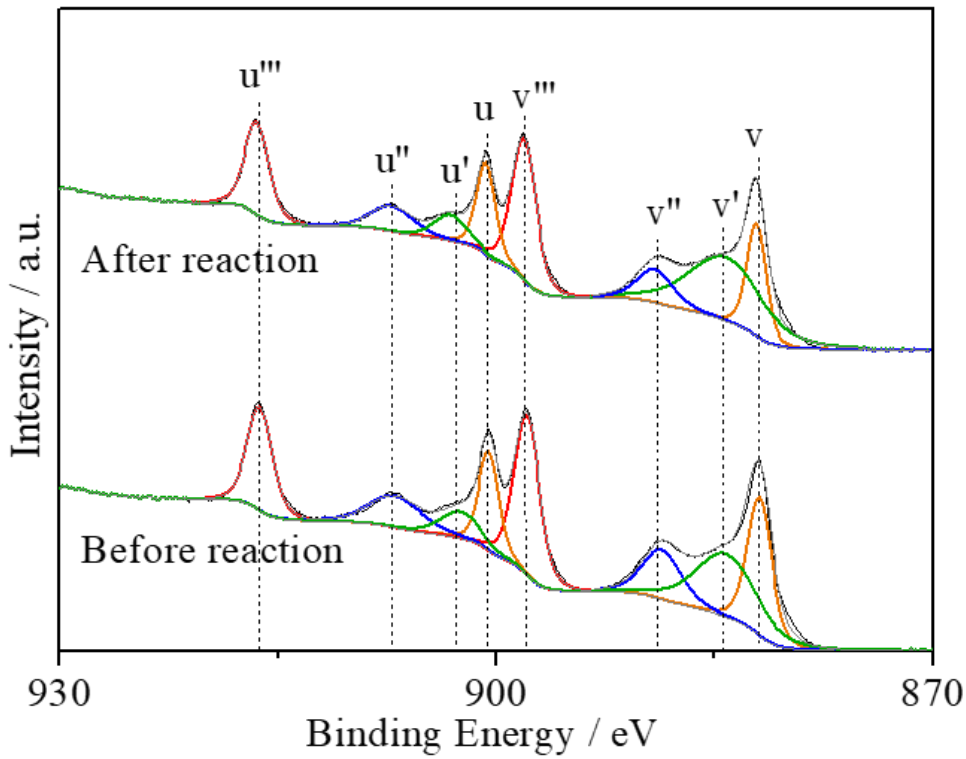

Figure. 3-5. XP spectra for Ce 3d of Fe_2O_3(3)/CeO_2 before and after reaction.

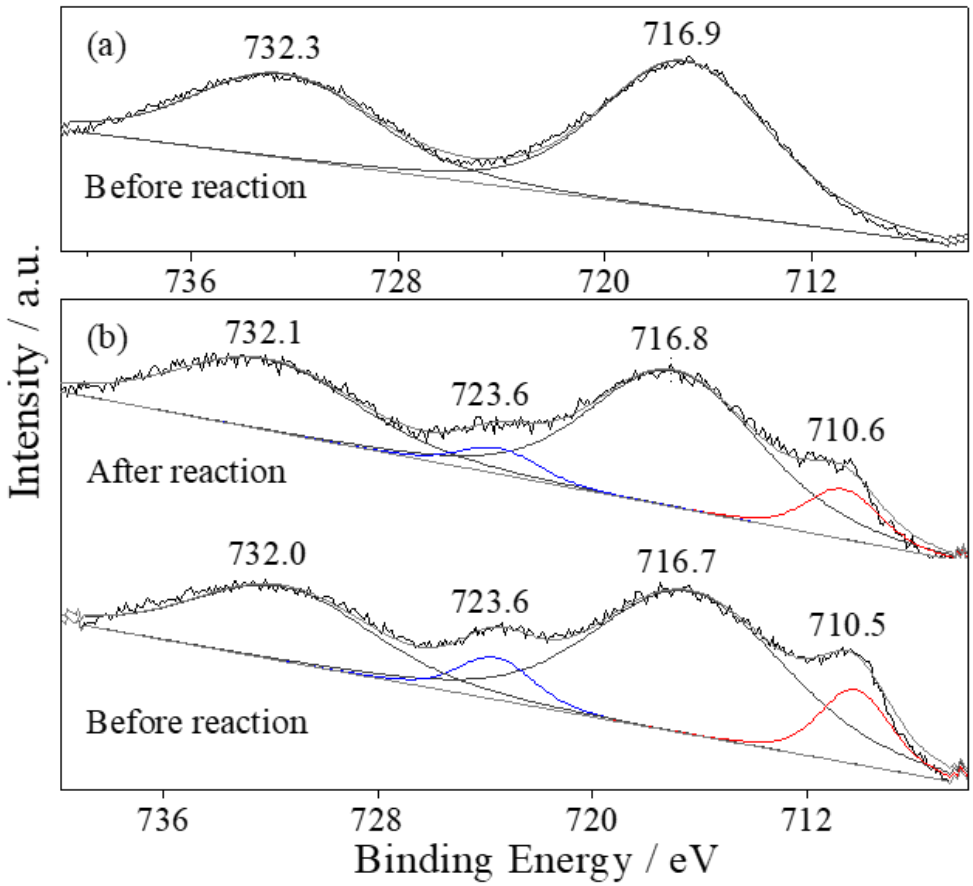

Figure. 3-6. XP spectra in Fe 2p region of (a) CeO_2 and (b) Fe_2O_3(3)/CeO_2.

3.3. BET

The specific surface area of fresh and used catalysts are given in Table 1. CeO_2 has a specific surface area of 132 m^2/g and a sharp decrease to 89 m^2/g is observed as 1.5 wt% Fe is added. However, the difference in specific surface area according to the loading amount of Fe is not so remarkable. A decrease in surface area is observed after the reaction in all samples, but the greatest change occurs in pure CeO_2.

Table 1.

The specific surface area of fresh and used catalysts.

Sample	BET area (m^2/g)	
CeO_2	132	71
Fe_2O_3(1.5)/ CeO_2	89	53
Fe_2O_3(3)/ CeO_2	87	56
Fe_2O_3(4)/ CeO_2	80	55
Fe_2O_3(6)/ CeO_2	78	50

3.4. XRD

XRD patterns of fresh and used CeO_2 samples are shown in Figure. 3-7. At all temperature range, cubic fluorite structure (JCPDS 34-0394, Fm3m) of cerium oxide is maintained. As shown in Figure. 3-8, the peaks in XRD patterns of all fresh samples with different Fe loading are also assigned to the cubic fluorite structure of cerium oxide [36, 43-45]. There are no peaks assigned to iron oxide phases, implying that no crystalline iron oxides are formed due to the fine dispersion or the formation of Fe-Ce solid solution. In addition, as can be seen in Figure. 3-9, the peak assigned to cerium oxide (1 1 1) shifts to higher angle with introducing Fe into CeO_2, which can reaffirm the formation of Fe-Ce solid solution [35]. The unit lattice parameters of cerium oxide calculated with the (1 1 1) peak are summarized in Table 2. As the iron loading amount increases from 0 to 3 wt%, the decrease of the unit cell lattice parameter from 5.390 Å to 5.357 Å is observed with the shift of the peak corresponding to cerium oxide (1 1 1) (Table 2 and Figure. 3-9). The unit cell shrinkage is caused by the substitution of large Ce^{4+} (1.01 Å) with small Fe^{3+} (0.64 Å) [35, 46]. However, there is no significant difference between the unit cell lattice parameter of cerium oxide in

Fe_2O_3(3)/CeO_2 and Fe_2O_3(4)/CeO_2. Hence it seems to that the concentration of iron in cerium oxide lattice comes to saturation point or that the iron solubility into cerium oxide decreases because of the agglomeration of iron. The latter is more reasonable because the decrease of the angle corresponding to the (1 1 1) and the increase of the unit cell lattice parameter are confirmed with increasing of iron content from 4 wt% to 6 wt% which means a reduction in the iron amount forming Fe–Ce solid solution.

The crystallite size of samples calculated with the reflections of cerium oxide (1 1 1) using the Scherrer's equation are displayed in Table 2. Fresh CeO_2 and Fe_2O_3(1.5)/CeO_2 samples have crystallite size of 10.4 nm and 10.0 nm, respectively, whereas those of used samples are 17.4 nm and 13.4 nm. On the other hand, no significant difference is observed between the crystallite size of cerium oxide phase in fresh and used samples of Fe_2O_3(x)/CeO_2 (x=3, 4 and 6). In other words, during the oxidative chlorination of methane, the sintering of cerium oxide catalysts is markedly inhibited by the introducing of Fe.

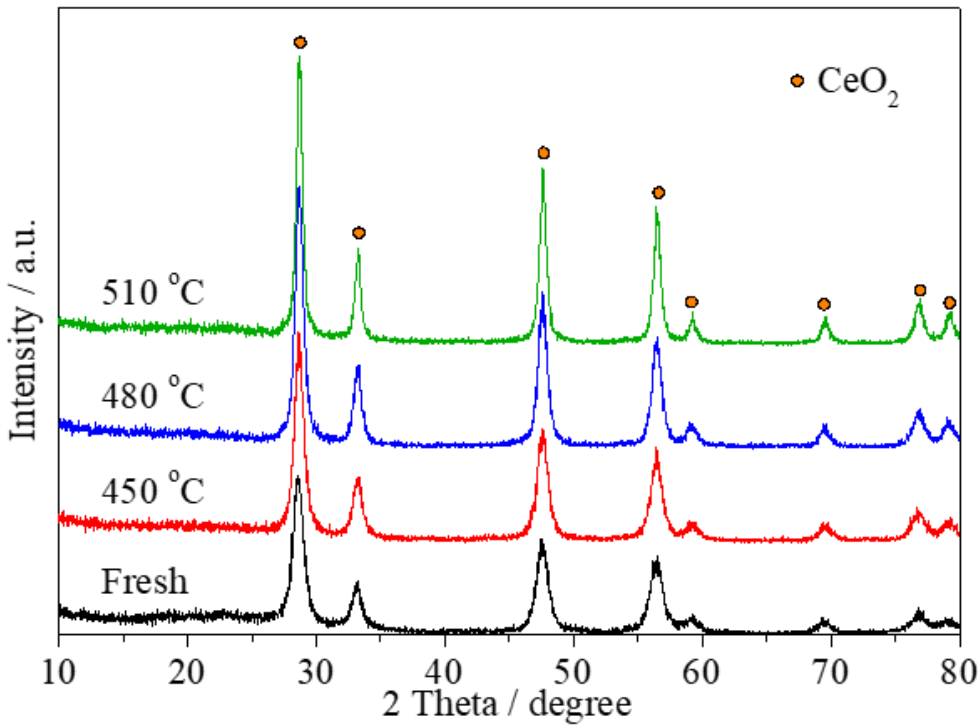

Figure. 3-7. XRD patterns of CeO_2 before and after reaction at 450, 480 and 510 ℃.

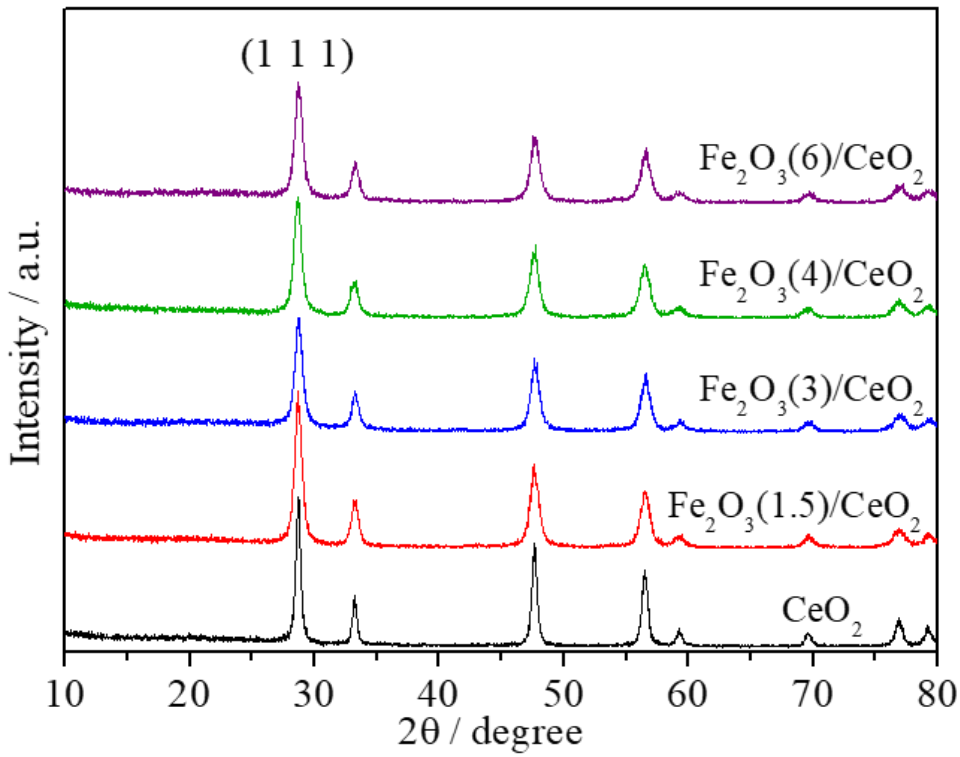

Figure. 3-8. XRD patterns of $Fe_2O_3(x)/CeO_2$ before reaction.

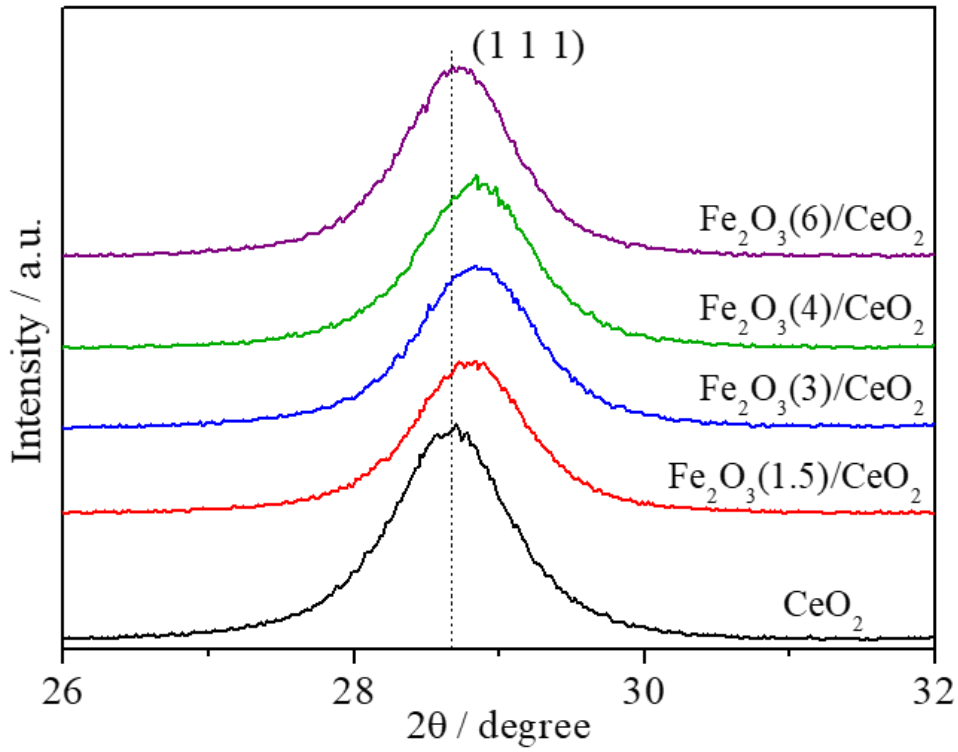

Figure. 3-9. Fine scanning XRD patterns of Fe_2O_3(x)/CeO_2 before reaction in the 2θ ranges of 26-32°.

Table 2.

Textural properties of the catalysts with different Fe loading.

Sample	Crystalline size (nm)		a^a (Å)
	Fresh	Used at 510 ℃	
CeO_2	10.4	17.4	5.390
$Fe_2O_3(1.5)/CeO_2$	10.0	13.4	5.366
$Fe_2O_3(3)/CeO_2$	10.4	12.1	5.357
$Fe_2O_3(4)/CeO_2$	10.1	12.4	5.358
$Fe_2O_3(6)/CeO_2$	10.7	12.4	5.381

[a] unit cell lattice parameter of cerium oxide in fresh samples

3.5. TEM

Figure. 3-10 shows TEM images used to measure the average crystallite size of ceria in the fresh and used samples. The ceria-based average crystallite size in the CeO_2 sample is almost doubled from 9.4 nm to 17.8 nm after the reaction at 510 ℃. However, in Fe_2O_3(3)/CeO_2, the ceria based average crystallite size of 10.0 nm before the reaction and 12.7 nm after the reaction at 510 ℃ are obtained. These are consistent with the results that the addition of Fe prevents catalyst sintering during the reaction identified by XRD.

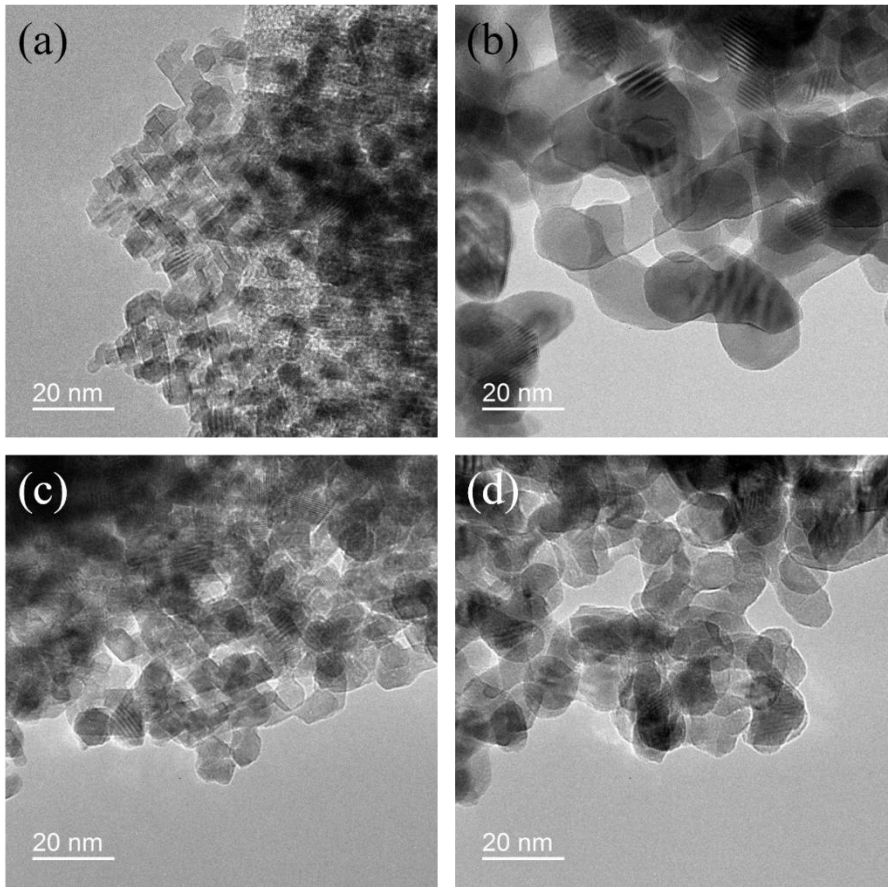

Figure. 3-10. TEM images of CeO_2 (a) fresh, (b) after reaction at 510 ℃ and Fe_2O_3(3)/CeO_2 (c) fresh, (d) after reaction at 510 ℃.

3.6. H_2 TPR

H_2 temperature programmed reduction (H_2 TPR) was carried out to investigate the reduction properties of the catalysts. It is known that there are two reduction peaks of cerium oxide at 300–600 ℃ and 700–1000 ℃, which are corresponded to the surface reduction and bulk reduction of cerium oxide, respectively [44, 47]. Two discrete peaks can be distinguished in the reduction temperature range of surface cerium oxide. The reduction peak of surface adsorbed oxygen is observed at relatively low temperature and that of surface lattice oxygen appears at relatively high temperature [35, 48]. Iron oxide has a total of three possible reduction steps at 340 ℃ ($Fe_2O_3 \rightarrow Fe_3O_4$), 630 ℃ ($Fe_3O_4 \rightarrow FeO$) and 705 ℃ ($FeO \rightarrow Fe$) [35].

Figure. 3-11 shows the H_2 TPR profiles of fresh samples. The peaks of bulk cerium oxide reduction are observed at similar temperature regions (750–950 ℃) in all samples. On the other hand, the peaks corresponding to the reduction of the surface cerium oxide shift to a lower temperature as the iron content increases from 0 to 3 wt%. The shift of peaks can be explained in that the Ce–O bond is weakened by a small amount of iron introduced into cerium oxide and that the oxygen vacancy concentration in cerium oxide lattice is

increased by a charge compensating mechanism [35, 49, 50]. However, when a large amount of iron, over 3 wt%, is added to the cerium oxide lattice, the reducibility of the catalyst is rather deteriorated. This is due to the elimination of the oxygen vacancy which contributes to that the iron occupies the interstitial site of cubic fluorite lattice (interstitial compensation mechanism) or forms coalesce itself (diminution of charge compensation effect) [35, 49]. The agglomeration of iron, identified in 3.4. XRD, is also confirmed by the peaks at 600–750 ℃, which are assigned as Fe_3O_4 reduction to Fe, in the H_2 TPR profiles of Fe_2O_3(4)/CeO_2 and Fe_2O_3(6)/CeO_2 [35, 51]. It is noted that the Fe_2O_3(3)/CeO_2 where the yield of chlorinated products is maximized has the reduction peak at lowest temperature.

The rate of elementary reaction in oxidative chlorination of methane is known as HCl oxidation>methane chlorination>DCM and methane oxidation [29]. In other words, the CM consumption rate via oxidation or further chlorination is considerably lower than the CM production rate. In addition, the reduced concentration of O_2 due to the fast HCl oxidation gives rise to the suppression of the further CM oxidation [29], and thus, high selectivity of CM is achieved over CeO_2 [3, 23, 29, 30]. The most energy-challenging step in HCl oxidation

is the Cl atom activation controlled by the cerium redox cycle [32, 33], so reducibility of surface cerium plays an important role in HCl activation [23, 30]. Therefore, it can be concluded that the HCl oxidation step is facilitated by the addition of Fe to increase reducibility of CeO_2, whereby the higher selectivity of CM and the lower selectivity of by-products are achieved over Fe_2O_3/CeO_2 than over CeO_2.

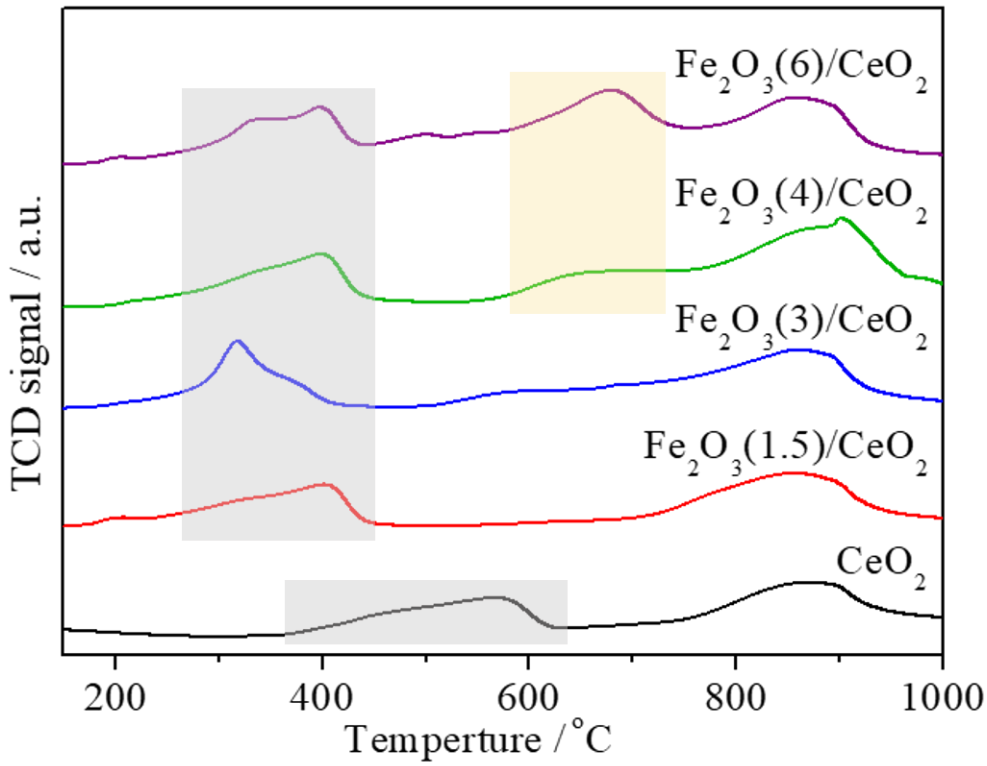

Figure. 3-11. H_2 TPR profiles of the fresh Fe_2O_3(x)/CeO_2 samples.

Chapter 4. Conclusion

In this work, methane oxychlorination was performed over metal/CeO_2 catalysts. Among the various metals, iron shows the best promotion effect on CeO_2 during the reaction. The CM yield is maximized at 510 ℃ where the conversion of methane and the selectivity of CM are obtained as 23% and 65%, respectively, over Fe_2O_3/CeO_2 with 3 wt% iron. The crystallite size of cerium oxide phase in fresh and used catalysts calculated by using XRD patterns and TEM images imply that the addition of iron suppresses the catalyst sintering during the reaction through the formation of iron–cerium solid solution which is detected by XRD and H_2 TPR. Moreover, the incorporated iron facilitates the reduction of cerium oxide, resulting in the promoted HCl oxidation rate, especially on Fe_2O_3(3)/CeO_2. In summary, Fe_2O_3(3)/CeO_2 exhibits the maximum yield of chlorinated products (CM+DCM+TCM) which is explicated by the increased cerium oxide reducibility, arising from the formation of iron–cerium solid solution.

References

[1] M. Ravi, M. Ranocchiari, J.A. van Bokhoven, A Critical Assessment of the Direct Catalytic Oxidation of Methane to Methanol, Angew. Chem. Int. Ed., (2017)16464-16483.

[2] B. Wang, S. Albarracín-Suazo, Y. Pagán-Torres, E. Nikolla, Advances in methane conversion processes, Catal. Today, 285 (2017) 147-158.

[3] W. Taifan, J. Baltrusaitis, CH_4 conversion to value added products: Potential, limitations and extensions of a single step heterogeneous catalysis, Appl. Catal. B Environ., 198 (2016) 525-547.

[4] R. Horn, R. Schlögl, Methane activation by heterogeneous catalysis, Catal. Lett., 145 (2015) 23-39.

[5] Q. Zhu, X. Zhao, Y. Deng, Advances in the partial oxidation of methane to synthesis gas, J. Nat. Gas Chem., 13 (2004) 191-203.

[6] Z. Li, G.B. Hoflund, A review on complete oxidation of methane at low temperatures, J. Nat. Gas Chem., 12 (2003) 153-160.

[7] U.S. Energy Information Administration, International Energy Outlook 2016, (2016).

[8] P. Schwach, X. Pan, X. Bao, Direct conversion of methane to

value-added chemicals over heterogeneous catalysts: challenges and prospects, Chem. Rev., 117 (2017) 8497-8520.

[9] E. McFarland, Unconventional Chemistry for Unconventional Natural Gas, Science, 338 (2012) 340-342.

[10] P. Gélin, M. Primet, Complete oxidation of methane at low temperature over noble metal based catalysts: A review, Appl. Catal. B Environ., 39 (2002) 1-37.

[11] S.G. JPodkolzin, E.E. Stangland, M.E. Jones, E. Peringer, J.A. Lercher, Methyl chloride production from methane over lanthanum-based catalysts, J. Am. Chem. Soc., 129 (2007) 2569-2576.

[12] J. Chen, H. Arandiyan, X. Gao, J. Li, Recent Advances in Catalysts for Methane Combustion, Catal. Surv. Asia, 19 (2015) 140-171.

[13] B. Han, Y. Yang, Y. Xu, U.J. Etim, K. Qiao, B. Xu, Z. Yan, A review of the direct oxidation of methane to methanol, Cuihua Xuebao/Chinese J. Catal., 37 (2016) 1206-1215.

[14] U.S. Energy Infromation Administration, Monthly Energy Review, September 2017, (2017).

[15] V. Paunović, G. Zichittella, M. Moser, A.P. Amrute, J. Pérez-Ramírez, Catalyst design for natural-gas upgrading through

oxybromination chemistry, Nat. Chem., 8 (2016) 803-809.

[16] C. Li, G. Zhou, L. Wang, Z. Li, Y. Xue, T. Cheng, Effect of impregnation procedure of La_2O_3 precursor on copper-based catalysts for ethane oxychlorination, Catal. Commun., 13 (2011) 22-25.

[17] Z. Li, G. Zhou, C. Li, T. Cheng, Effect of Pr on copper-based catalysts for ethane oxychlorination, Catal. Commun., 40 (2013) 42-46.

[18] V. Paunović, G. Zichittella, R. Verel, A.P. Amrute, J. Pérez-Ramírez, Selective production of carbon monoxide via methane oxychlorination over vanadyl pyrophosphate, Angew. Chem. Int. Ed., 55 (2016) 15619-15623.

[19] E. Peringer, C. Tejuja, M. Salzinger, A.A. Lemonidou, J.A. Lercher, On the synthesis of $LaCl_3$ catalysts for oxidative chlorination of methane, Appl. Catal. A Gen., 350 (2008) 178-185.

[20] E. Peringer, S.G. Podkolzin, M.E. Jones, R. Olindo, J.A. Lercher, $LaCl_3$-based catalysts for oxidative chlorination of CH_4, Top. Catal., 38 (2006) 211-220.

[21] V. Paunovic, G. Zichittella, S. Mitchell, R. Hauert, J. Pérez-Ramírez, Selective Methane Oxybromination over Nanostructured

Ceria Catalysts, ACS Catal., 8 (2017) 291–303.

[22] V. Paunović, M. Artusi, R. Verel, F. Krumeich, R. Hauert, J. Pérez–Ramírez, Lanthanum vanadate catalysts for selective and stable methane oxybromination, J. Catal., 363 (2018) 69–80.

[23] R. Lin, A. Amrute, J. Pérez–Ramírez, Halogen–mediated conversion of hydrocarbons to commodities, Chem. Rev., 117 (2017) 4182–4247.

[24] V. Paunović, R. Lin, M. Scharfe, A.P. Amrute, S. Mitchell, R. Hauert, J. Pérez–Ramírez, Europium oxybromide catalysts for efficient bromine looping in natural gas valorization, Angew. Chem. Int. Ed., 56 (2017) 9923–9927.

[25] R. Lin, Y. Ding, L. Gong, J. Li, W. Chen, L. Yan, Y. Lu, Oxidative bromination of methane on silica–supported non–noble metal oxide catalysts, Appl. Catal. A Gen., 353 (2009) 87–92.

[26] G. Zichittella, B. Puértolas, V. Paunović, T. Block, R. Pöttgen, J. Pérez–Ramírez, Halogen type as a selectivity switch in catalysed alkane oxyhalogenation, Catal. Sci. Technol., 8 (2018) 2231–2243.

[27] M. Scharfe, M. Capdevila–Cortada, V.A. Kondratenko, E.V. Kondratenko, S. Colussi, A. Trovarelli, N. López, J. Pérez–Ramírez,

Mechanism of ethylene oxychlorination on ceria, ACS Catal., (2018) 2651-2663.

[28] Z. Vajglová, N. Kumar, K. Eränen, A. Tokarev, M. Peurla, J. Peltonen, D.Y. Murzin, T. Salmi, Influence of the support of copper catalysts on activity and 1, 2-dichloroethane selectivity in ethylene oxychlorination, Appl. Catal. A Gen., 556 (2018) 41-51.

[29] G. Zichittella, V. Paunovic, A.P. Amrute, J. Pérez-Ramírez, Catalytic oxychlorination versus oxybromination for methane functionalization, ACS Catal., 7 (2017) 1805-1817.

[30] J. He, T. Xu, Z. Wang, Q. Zhang, W. Deng, Y. Wang, Transformation of methane to propylene: A two-step reaction route catalyzed by modified CeO_2 nanocrystals and zeolites, Angew. Chem. Int. Ed., 51 (2012) 2438-2442.

[31] A.P. Amrute, C. Mondelli, M.A.G. Hevia, J. Pérez-Ramírez, Mechanism-performance relationships of metal oxides in catalyzed HCl oxidation, ACS Catal., 1 (2011) 583-590.

[32] A.P. Amrute, C. Mondelli, M. Moser, G. Novell-Leruth, N. López, D. Rosenthal, R. Farra, M.E. Schuster, D. Teschner, T. Schmidt, Performance, structure, and mechanism of CeO_2 in HCl oxidation to Cl_2, J. Catal., 286 (2012) 287-297.

[33] M. Capdevila-Cortada, G. Vilé, D. Teschner, J. Pérez-Ramírez, N. López, Reactivity descriptors for ceria in catalysis, Appl. Catal. B Environ., 197 (2016) 299-312.

[34] L.-L. Yin, G. Lu, X.-Q. Gong, A DFT+U study on the oxidative chlorination of CH_4 at Ceria: the role of HCl, Catal. Sci. Technol., (2017)2498-2505.

[35] W. Wang, Q. Zhu, F. Qin, Q. Dai, X. Wang, Fe doped CeO_2 nanosheets as Fenton-like heterogeneous catalysts for degradation of salicylic acid, Chem. Eng. J., 333 (2018) 226-239.

[36] A.S. Reddy, C.-Y. Chen, C.-C. Chen, S.-H. Chien, C.-J. Lin, K.-H. Lin, C.-L. Chen, S.-C. Chang, Synthesis and characterization of Fe/CeO_2 catalysts: Epoxidation of cyclohexene, J. Mol. Catal. A Chem., 318 (2010) 60-67.

[37] Y. Jiang, C. Bao, Q. Liu, G. Liang, M. Lu, S. Ma, A novel CeO_2-MoO_3-WO_3/TiO_2 catalyst for selective catalytic reduction of NO with NH_3, Catal. Commun., 103 (2018) 96-100.

[38] T. Yamashita, P. Hayes, Analysis of XPS spectra of Fe^{2+} and Fe^{3+} ions in oxide materials, Appl. Surf. Sci., 254 (2008) 2441-2449.

[39] S. Roosendaal, B. Van Asselen, J. Elsenaar, A. Vredenberg, F. Habraken, The oxidation state of Fe (100) after initial oxidation in O_2, Surf. Sci., 442 (1999) 329-337.

[40] P.C. Graat, M.A. Somers, Simultaneous determination of composition and thickness of thin iron-oxide films from XPS Fe 2p spectra, Appl. Surf. Sci., 100 (1996) 36-40.

[41] P. Mills, J. Sullivan, A study of the core level electrons in iron and its three oxides by means of X-ray photoelectron spectroscopy, J. Phys. D Appl Phys., 16 (1983) 723-732.

[42] Thermo Fisher Scientific Inc., http://xpssimplified.com/elements/iron,php (accessed 22 January 2018).

[43] Z. Cui, J. Fan, H. Duan, J. Zhang, Y. Xue, Y. Tan, Effect of calcination atmospheres on the catalytic performance of nano-CeO_2 in direct synthesis of DMC from methanol and CO_2, Kor. J. Chem. Eng., 34 (2017) 29-36.

[44] M.F. Mohamad, A. Ramli, S. Yusup, Study on the physicochemical properties of Fe/CeO_2 catalysts as an effect from different iron loading, AIP Conf. Proc., 1502 (2012) 288-297.

[45] L. Kongzhai, W. Hua, W. Yonggang, L. Mingchun, Preparation and characterization of Ce1-xFe_xO_2 complex oxides and its catalytic activity for methane selective oxidation, J. Rare Earths, 26 (2008) 245-249.

[46] F. Pérez-Alonso, M. López Granados, M. Ojeda, P. Terreros, S. Rojas, T. Herranz, J. Fierro, M. Gracia, J. Gancedo, Chemical

structures of coprecipitated Fe−Ce mixed oxides, Chem. Mater., 17 (2005) 2329-2339.

[47] Y. Li, B. Zhang, X. Tang, Y. Xu, W. Shen, Hydrogen production from methane decomposition over Ni/CeO_2 catalysts, Catal. Commun., 7 (2006) 380-386.

[48] Q. Shen, L. Zhang, N. Sun, H. Wang, L. Zhong, C. He, W. Wei, Y. Sun, Hollow MnO_x-CeO_2 mixed oxides as highly efficient catalysts in NO oxidation, Chem. Eng. J., 322 (2017) 46-55.

[49] W. Cai, F. Chen, X. Shen, L. Chen, J. Zhang, Enhanced catalytic degradation of AO7 in the CeO_2-H_2O_2 system with Fe^{3+} doping, Appl. Catal. B Environ., 101 (2010) 160-168.

[50] A. Trovarelli, Structural and oxygen storage/release properties of CeO_2-based solid solutions, Comm. Inorg. Chem., 20 (1999) 263-284.

[51] L. Tang, D. Yamaguchi, N. Burke, D. Trimm, K. Chiang, Methane decomposition over ceria modified iron catalysts, Catal. Commun., 11 (2010) 1215-1219.

요약 (국문 초록)

천연가스 구성성분의 대부분을 차지하는 메탄은 석유를 대체할 수 있는 풍부한 자원이다. 그러나 메탄은 매우 안정한 4개의 C-H 결합으로 이루어져 있기 때문에 메탄의 효율적인 이용, 특히 화학물질 생산에의 이용은 촉매 분야에서 도전적인 과제로 연구되어 왔다. 수증기 개질, 부분산화 그리고 자열 개질 등 상용화 된 메탄 활성화 공정들이 존재하지만, 그 공정들 모두 에너지, 자본 집약적이라는 단점이 있다.

반면, 산화 염소화 반응을 통한 메탄의 활성화는 상압 그리고 450-550 ℃의 온도범위의 상대적으로 온화한 반응 조건에서 진행되기 때문에 주목을 받고 있다. 메탄의 산화 염소화 반응에서 CeO_2가 자유로운 산화환원 ($Ce^{4+} \leftrightarrow Ce^{3+}$) 특성을 통해 좋은 활성을 나타내는 것으로 알려져 있으나, 반응 중 주 생성물인 클로로메탄, 다이클로로메탄 외에도 상당한 양의 부반응 생성물이 (CO_2, CO 등) 생산된다. 실제 실험 결과 염소화 생성물의 수율이 최대가 되는 510 ℃에서 23%의 메탄 전환율, 56.8% 의 클로로메탄 선택도 그리고 17.2%의 다이클로로메탄 선택도가 얻어졌으나, 동시에 부산물이 약 26%의 선택도로 생성되었다.

본 연구에서는, CeO_2에 다양한 금속들을 담지 해 봄으로써 메탄의 산화 염소화 반응에 대한 CeO_2의 활성을 증진시키고자 하였다. 촉매는 습윤함침법으로 제조하였고 모든 촉매를 600 ℃에서 6시간 동안 소성하였

다. 반응 실험 결과 다양한 금속 중 철이 메탄의 산화 염소화 반응에 대한 CeO_2의 활성에 가장 좋은 증진 효과를 나타냈고, 그에 따라 Fe_2O_3/CeO_2 촉매에서 철의 영향을 좀 더 깊이 살펴보았다. 다양한 함량으로 철을 담지하여 실험 해 본 결과, 메탄의 전환율 측면에서는 철 담지의 장점이 없었지만 철이 담지 된 모든 촉매에서 철의 함량에 관계 없이 부반응 생성물의 생성이 억제되었다. 특히 3 중량%의 철이 담지 되었을 때 510 ℃에서 23% 메탄 전환율, 65% 클로로메탄 선택도로 최대 염소화 생성물 수율이 얻어졌다. 철을 담지 함으로써 반응성이 증대되는 원인을 알아보고자 XPS, BET, XRD, TEM 그리고 H_2 TPR과 같은 촉매 분석을 진행하였다. XRD와 H_2 TPR 분석 결과 철-세륨 고용체 형성이 확인되었고, 그 결과 CeO_2의 환원성이 증가하였다. 또한 반응 중 촉매 소결이 철을 담지 함으로써 억제 된다는 것을 XRD 그리고 TEM 결과를 통해 확인하였다. 결과적으로, CeO_2에 철을 담지 하면 촉매의 환원성이 증가하고 반응 중 HCl 산화가 촉진된다. 그에 따라 염소화 생성물의 선택성이 증가하고, 촉진된 HCl의 산화로 낮아진 반응물 중 산소 농도로 인해 염소화 생성물의 CO_2와 CO로의 추가적인 산화가 억제되어서 부산물의 선택도가 낮아지는 결과를 얻을 수 있었다.

주요어 : 메탄 활성화, 산화 염소화 반응, CeO_2, CO와 CO_2 생성 억제, 클로로메테인.

학 번 : 2016-21017